Master Thesis

Uncertainty Quantification and Sensitivity Analysis of Hemodynamic Indices for A Stenotic Coronary Artery

The Graduate School
of the University of Ulsan
Department of Mechanical Engineering

Nguyen Ho Nghia

Uncertainty Quantification and Sensitivity Analysis of Hemodynamic Indices for A Stenotic Coronary Artery

Supervisor: Sang-Wook Lee

A Dissertation

Submitted to
The Graduate School of the University of Ulsan
In partial Fulfillment of the Requirements
For the Degree of

Master of Science

by

Nguyen Ho Nghia

Department of Mechanical Engineering
Ulsan, Korea
August 2021

Uncertainty Quantification and Sensitivity Analysis
of Hemodynamic Indices for A Stenotic Coronary Artery

This certifies that the thesis of Nguyen Ho Nghia is approved

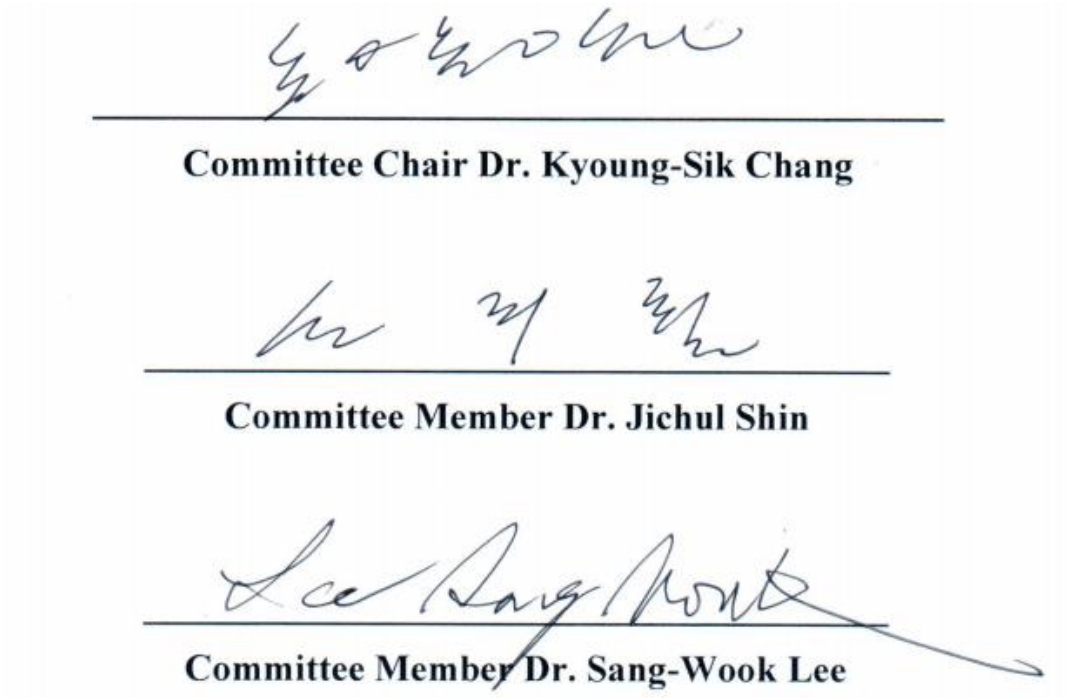

Committee Chair Dr. Kyoung-Sik Chang

Committee Member Dr. Jichul Shin

Committee Member Dr. Sang-Wook Lee

Department of Mechanical Engineering
Ulsan, Korea
August 2021

ACKNOWLEDGMENT

First of all, I am very grateful to Professor Sang-Wook Lee for his sincere advice, invaluable knowledge, and encouragement to complete my master's program at the University of Ulsan.

I am fortunate that I have an amazing family, with their endless support, I overcame difficulties to complete this 2-year journey.

I would like to thank my "big brother" Cheng Kui Yu for his care and support from the early days and throughout later studies.

I would also like to thank all my friends who have accompanied and shared with me the past journey, especially Khanh Hoan Nguyen, who has always encouraged me in the most difficult times.

I also take this opportunity to express a deep sense of gratitude to all employees and professors at the Mechanical and Automotive Engineering Department for their wonderful work.

ABSTRACT

In clinical, fractional flow reserve (FFR) and wall shear stress (WSS) are useful for assessing the severity of atherosclerosis. The computational fluid dynamics (CFD) method to access these indices is widely used, however, the uncertainty of the CFD prior parameters made it is not straightforward to predict, there are many sources of uncertainty, as the accuracy in vivo measurement. In this study, we conducted uncertainty quantification (UQ) and sensitivity analysis (SA) for an idealized stenotic coronary. By using the non-intrusive Point-Collocation method under helping of Chaospy software combined with a 3D-0D coupled P2P1 finite element solver. We applied these methods in terms of ideal conditions, with the assumption that blood vessels are rigid walls and blood flow is a Newtonian fluid. Two different models were considered: single stenosed vessel and tandem stenosed vessel with mean values for UQ and SA are taken from reliable sources. The UQ and SA results were expressed into expected and standard deviation values of the quantities of interest. These results show that UQ and SA are necessary when a small error in uncertain input (5% or 10%) can lead to a big change in output (can up to 20% in centerline velocity of the tandem stenosed vessel case), make the wrong decision. This study helps us understand the effect of different inputs on the hemodynamic indices of the stenotic coronary.

Keywords: Stenosed vessel, Hemodynamics, Uncertainty Quantification (UQ), Sensitivity Analysis (SA), non-intrusive Point-Collocation, Computational fluid dynamics (CFD)

TABLE OF CONTENTS

LIST OF FIGURES

LIST OF TABLES

1. INTRODUCTION

1.1 Coronary artery disease

Coronary artery disease (CAD, also called coronary heart disease or CHD) is the leading cause of global death [1], which is caused by the formation of atherosclerosis in the arteries that supply the heart with oxygen.

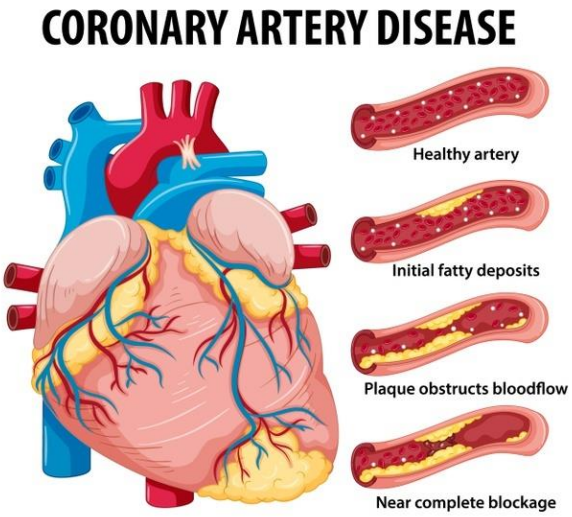

Figure 1.1 Coronary artery disease

The arteries are smooth and elastic, but when plaque appears on the inner wall of the artery, they change into stiff and narrow, blocking blood flow to the heart muscle or brain, leading to chest pain or headache.

In clinical cardiology, cardiologists quantify the significance of CAD by employing anatomical parameters of diameter stenosis (DS), area stenosis (AS), and hemodynamic indices of coronary flow reserve (CFD) and fractional flow reserve (FFR). These clinical parameters can be evaluated by invasive or non-invasive imaging techniques, such as coronary angiography, intravascular ultrasound (IVUS), computed tomography (CT),

magnetic resonance imaging (MRI), positron emission tomography (PET), and transthoracic echocardiography (TTE). With the rapid development of technology, anatomical images are valuable because of their high accuracy and low cost. However, this technique is based solely on anatomical features and does not provide complete hemodynamic information of the stenosis. Hemodynamic information such as blood flow and pressure of the coronary vascular beds are crucial to diagnose the quality of the coronary, along with the anatomic image. The FFR can be assessed using a catheter inserted into the femoral (groin) or radial arteries (wrist) using a sheath and guidewire. A small sensor on the tip of the wire to measure pressure, temperature, and flow to determine the severity of the lesion. However, this method is highly invasive and complex, and depends on the patient situation.

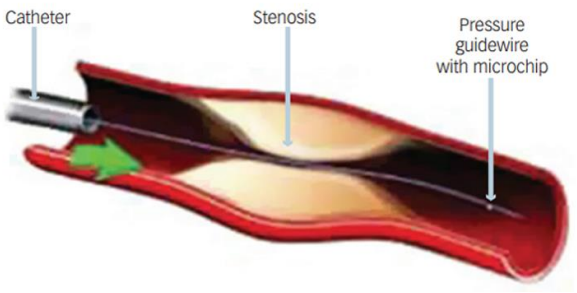

Figure 1.2 Measure pressure differences across coronary artery stenosis by using catheterization

Consequently, with the development of computer resources and mathematical models, computational fluid dynamics (CFD) is emerged as an alternative method to evaluate hemodynamic parameters, in conjunction with noninvasive and invasive imaging techniques. CFD uses numerical methods to solve the set of governing equations (usually continuity and Navier–Stokes's equations for single-phase blood flow). A general boundary condition in CFD simulation is velocity flow at inlets and pressure at outlets. Another computational model to mimic the blood flow is lumped parameter network (LPN) model, which is inspired

by the concept of hydraulic-electrical analog. LPN model is the 0D model, whereas the pressure and flow rate at the upstream or downstream region are assumed spatially uniform distribution at any time point. More particularly, the relationship of the pressure and flow rate at the upstream and downstream of the vasculature in LPN model is represented as impedance R, capacitance C, and inductance L. These parameters are the consequence of viscous friction, vessel wall elasticity, and blood flow inertia. This multiscale simulation is suitable for investigating CAD hemodynamics, since the impedance R can be calculated by dividing the vascular pressure by the blood flow rate, while the capacitance of the downstream is adjusted to mimic the phase of actual blood flow.

Based on these properties by LPN model, Sankaran et al. [2], Kim et al. [3] conducted the computational simulation of the hemodynamic properties in coronary arteries with the LPN model coupled finite element method. In these studies, the inflow in the aorta was generated by the lumped-parameter heart model, while the outlets of the branch vessels and thoracic aorta were coupled with the Windkessel models. In this way, the realistic blood flow in coronary arteries can be mimicked using CFD, therefore, the hemodynamics can be evaluated. Independent CFD studies of blood flow in coronary with different diameters of stenosis (DS) found that FFR is strongly dependent of DS and hyperemic vascular resistance [4].

In addition to the FFR to assess the condition of the coronary, another local hemodynamic force is the wall shear stress (WSS). WSS is the tangential friction force caused by the blood flow on the coronary wall, independent of the systemic factors, WSS has an important role in the generation, progression, and destabilization of the atherosclerotic plaques [5-7], while, atherosclerosis is the dominant factor leading to myocardial ischemia. Hence, WSS is considered as a important index in the diagnosis, the value of WSS is expressed in terms of dynes/cm^2, and its physiological values in the healthy arteries system are from 15 to 20 dynes/cm^2 [8]. The WSS values are divided into two ranges corresponding to different effects.

A high-WSS theory developed by Fry [9] in 1968 through in vitro experiments in the thoracic aorta of dogs asserted an abnormality when the time mean WSS was 379 ± 85 dynes/cm^2, and a high WSS is related to damage and denudate the endothelial cell, leading to the formation of the atherosclerotic plaque. On the other hand, the low-WSS theory established by Zarins et al. [10] in 1983 through in vitro experiments showed that the development of thickening on carotid bifurcations in the region of WSS < 6 dynes/cm^2. Low-WSS is estimated to prolonged and increase lipids at local regions, leading to the formation of atherosclerosis.

With the development of computational resources and numerical schemes, the hemodynamic indices can be validated straightforward. In addition to CFD studies, experimental approaches are also conducted. An example of an experimental setup for stenosis can be found in the study of Huh et al. [11]. The working blood in the experiment is prepared by mixing components to mimic properties of real blood, and coronary stenosis object is generated as idealized tandem stenosis. The flow rates in the experiment are corresponding to the Reynolds number of 185, 375, and 750. The degree of proximal and distal stenosis are considered as 50%-50% and 50%-75% They obtained interesting results on the interactions between proximal stenosis and distal stenosis such that the severity of the distal stenosis did not affect flow after proximal stenosis.

For applying physiological mathematical models to simulate the properties of the myocardial system, or using sophisticated equipment to measure hemodynamic parameters, a fact must be accepted that: the results have a certain confidence interval where the input parameters are uncertain due to the in vivo measurement or image processing techniques, etc. To make the model reliable and suitable for clinical decision-making, uncertainty quantification (UQ) and sensitivity analysis (SA) are therefore essential.

1.2 Uncertainty Quantification and Sensitivity analysis

Although computational simulation technology is widely applied to understand cardiovascular physiology, the precision, and accuracy of results are still big challenges. They are related not only to numerical techniques solving governing equations, but also to the uncertainty of input parameters. In this study, the uncertainty of the input parameters is of interest only because the accuracy of the simulation results can be easily improved if the accurate values of the input parameters are known.

All input measurement parameters are affected by the measurement uncertainty (because most of them are in vivo measurements which depends on the patient's condition), furthermore, not all input parameters are measurable (e.g., the resistance of coronary).

Not only one parameter is used as input in simulation models, but many different parameters are also used (e.g., blood flow rate and pressure used as boundary conditions, blood viscosity and density from personalized information and blood vessel morphology, etc...). The accuracy of the clinical prediction based on computational simulation can be improved by using more detailed vessel geometry or by using more patient-specific input parameters, but this also leads to an accumulation error because many input parameters must be accessed. Therefore, it is necessary to find the optimal point of the model, by using UQ and SA to evaluate which model inputs can be fixed to population-based and which must be accurately measured [12].

These are largely two methods in UQ and SA: local methods and global methods. While the local methods validate the uncertainty of output by changing infinitesimal around the mean value of one model input, the global methods consider all input parameters. Because of the complex relationship between the hemodynamic quantities, local methods are not applicable to assess the uncertainty of the output values, since they are non-addictive, non-monotonic, and non-linear.

The application of UQ and SA to the model for uncertainty analysis can be divided into two different methods based on how they have been conducted: the intrusive or non-intrusive method. The intrusive method will translate the uncertainty input parameters into the governing equations, then derive a new model. This method is complex and hard to implement widely [13]. However, the non-intrusive method does not require any changes in the CFD code. The deterministic code is treated as a black-box model and stochastic variable values are propagated into this model. The commonly used non-intrusive methods are Monte Carlo (MC) method [14], the non-intrusive polynomial chaos (NIPC) method [15], and the Lagrangian interpolation method [16].

MC method can be implemented easily, therefore, it is widely applied: create a random input sample set, then evaluate the whole set with a black-box code. The convergence rate of this method is completely independent of the number of dimensions, however, it strictly depends on the number of samples (law of large numbers). While the NIPC method will expand the output into a series of orthogonal polynomials based on a set of stochastic input parameters, it needs a smaller number of samples than the MC method [12], however, this method is not easy to implement as the MC method.

In 2015, Eck et al. [12] conducted a comparative study of MC and NIPC methods, thereby figured out the advantages and disadvantages of these methods. NIPC method with fourth-order polynomial and only 2,002 samples produced similar results as MC method with a total of 60,000 samples.

1.3 Objectives and Outline

In this study, we investigated the variance of WSS and FFR from computational simulation due to uncertain input parameters. For numerical technique to simulate blood flow dynamics in a coronary artery model, the finite element method coupled with lumped

parameters network model was used. Idealized single stenotic coronary was constructed based on geometrical characteristic parameters averaged from the left anterior coronary artery (LAD) population. In addition, the evaluation of the influence by the input parameters on outputs is conducted by SA, from which it is possible to distinguish which input parameters need to be improved in vivo measurement. For a tandem stenosis, we conducted FEM simulation with the same boundary conditions as the experiment of Huh et al. [11] for validation. Then, we performed UQ and SA using the NIPC method and assessed the influence of input parameters on the centerline velocity.

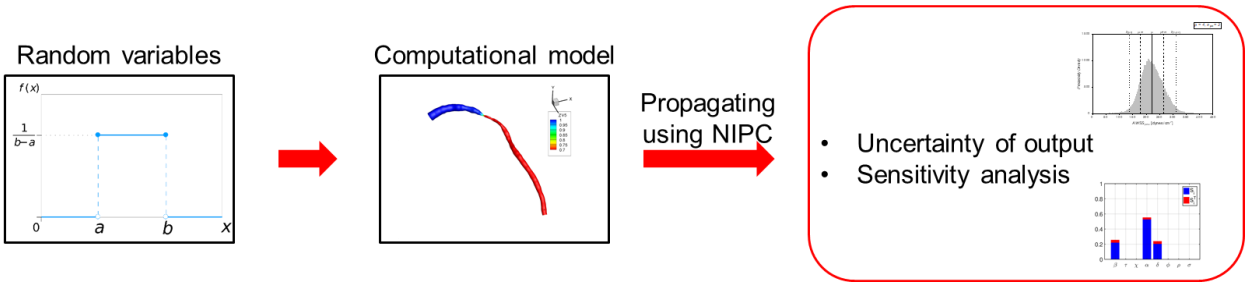

Figure 1.3 Uncertainty Quantification and Sensitivity Analysis process for coronary artery application

The thesis is divided into 4 sections. The first section introduces the background knowledge about CAD and objectives. The second section focuses on methods: UQ and SA technique, FEM coupled LPM, geometry modeling. Then in the third section, the UQ and SA results are presented. Finally, the fourth section is conclusion for this study.

2. METHOD

In this section, the basic concepts of the non-intrusive polynomial chaos method are presented in section 2.1, followed by the sensitivity analysis in section 2.2, the geometry of the idealized stenotic coronary and the uncertain variables in section 2.3, and eventually, the CFD model used for the computation in section 2.4.

2.1 Non-intrusive Polynomial Chaos

In the presentation of the non-intrusive polynomial chaos (NIPC) method, deterministic variable Y was denoted as output corresponding to n deterministic input variables $\boldsymbol{X} = (X_1, X_2, \dots, X_n)$ - by using a deterministic CFD code f.

$$Y = f(\boldsymbol{X}) \tag{2.1}$$

Using the polynomial chaos, a surrogate model is divided into separable deterministic and random components to replace the original model. This method is based on the spectral representation of the uncertainty [17]. The objective of the non-intrusive polynomial chaos is to determine the coefficients without changing the deterministic CFD code.

$$Y^* \approx \sum_{i=1}^{N_P} \alpha_i \Psi_i(\boldsymbol{X}) \tag{2.2}$$

where, Ψ_i is the expansion or polynomial, usually orthogonal polynomial concerning the probability distribution of inputs $\boldsymbol{X} = (X_1, X_2, \dots, X_n)$, α_i is the coefficient, and N_P is the total number of terms. In theory, the number of samples N_P should be infinite, however, the number of samples can be considered using the following equation based on the order of the polynomial and the number of dimensions:

$$N_p = \frac{(n+p)!}{n!p!} \tag{2.3}$$

Another approach to estimate the number of samples is proposed by Eldred et. al. [18], using the tensor product:

$$N_p = \prod_{i=1}^{n}(p_i + 1) \tag{2.4}$$

where p_i is the order of polynomial for the dimension i^{th}. The univariate polynomial is determined by the Wiener-Askey scheme [19]. For example, if the input variable has the normal distribution, the Hermite polynomial is used.

Using the product of univariate orthogonal polynomials, the multivariate basic functions can be evaluated. For example, multivariate Hermite polynomials can be evaluated by

$$H_n\left(X_{i_1}, \dots, X_{i_n}\right) = H_n\left(\vec{X}\right) = e^{\frac{1}{2}\boldsymbol{X}^T\boldsymbol{X}}(-1)^n \frac{\delta^n}{\delta X_{i_1} \dots \delta X_{i_n}} e^{-\frac{1}{2}\boldsymbol{X}^T\boldsymbol{X}} \tag{2.5}$$

The classical Wiener-Hermite polynomial chaos corresponding to the type of continuous probability distributions is described in Table 2.1.

Table 2.1 Wiener-Hermite polynomial chaos corresponding to the type of continuous probability distributions

Distribution of X	**Polynomial**	**Support**
Gaussian	Hermite	$(-\infty, \infty)$
Gamma	Laguerre	$[0, \infty)$
Beta	Jacobi	$[a, b]$
Uniform	Legendre	$[a, b]$

If the input parameters have a different probability distribution, then the multivariate basis function can be evaluated by optimal univariate polynomial at each random dimension.

The ultimate purpose of the stochastic methods based on NIPC is to evaluate the coefficient α_i in the polynomial expansion in equation (2.1). Using the NIPC method, these coefficients can be obtained without making a change to anything inside the deterministic CFD code.

There are two common NIPC methods to evaluate these coefficients: spectral projection NIPC (also called the pseudo-spectral approach and discrete projection) and regression NIPC method.

2.1.1 Spectral projection NIPC

Using the spectral projection NIPC (as known as pseudo-spectral approach and discrete projection), the coefficients α_i are determined based on spectral projection. In summary, the procedure for calculating coefficients by spectral projection can be listed as follows [20]:

- Generate nodes and weights from a quadrature integration scheme.
- Model predictions are created based on the generate nodes.
- Select polynomials Ψ_i.
- Calculate coefficients α_i.
- Analyze the surrogate model Y^*.

2.1.2 Regression NIPC

The regression method (also called the point-collocation method) replaces the output of a stochastic input set with the polynomial expansion. With the deterministic code, the solution can be obtained from the input set, then derives the linear problem:

$$\begin{pmatrix} \Psi_1(\boldsymbol{X}_1) & \Psi_2(\boldsymbol{X}_1) & \dots & \Psi_{N_p}(\boldsymbol{X}_1) \\ \Psi_1(\boldsymbol{X}_2) & \Psi_2(\boldsymbol{X}_2) & \dots & \Psi_{N_p}(\boldsymbol{X}_2) \\ \vdots & \vdots & \ddots & \vdots \\ \Psi_1\left(\boldsymbol{X}_{N_p}\right) & \Psi_2\left(\boldsymbol{X}_{N_p}\right) & \dots & \Psi_{N_p}\left(\boldsymbol{X}_{N_p}\right) \end{pmatrix} \begin{pmatrix} \alpha_1 \\ \alpha_2 \\ \vdots \\ \alpha_{N_p} \end{pmatrix} = \begin{pmatrix} Y_1 \\ Y_2 \\ \vdots \\ Y_{N_p} \end{pmatrix} \tag{2.6}$$

It is recommended to use the number of samples is twice more than the required in the equation (2.3) ($n_{ps} = 2$) to obtain a better approximation [15].

The convergence of the regression method is independent of the sampling method. However, the Hammersley sampling and Latin Hypercube sampling usually provide smoother convergence than random sampling.

2.2 Sensitivity Analysis

The equation (2.2) can be written as:

$$y = \Psi_0 + \sum_{i=1}^{n} \Psi_i(\xi_i) + \sum_{i<j}^{n} \Psi_{ij}(\xi_i, \xi_i) + \cdots + \Psi_{1,2,\ldots,n}(\xi_1, \xi_2, \ldots, \xi_n) \quad (2.7)$$

By using all the orthogonal equations:

- Expected (Mean) value

$$\mu[Y] = \mathbb{E}[Y] = \int_{\Omega_Y} y \rho_Y(y)\, dy \quad (2.8)$$

- Standard deviation

$$\sigma[Y] = \sqrt{\mathbb{V}[Y]} = \sqrt{\int_{\Omega_Y} (y - \mathbb{E}[Y])^2 \rho_Y(y)\, dy} \quad (2.9)$$

$$\mathbb{V}[Y] = \sum_{i=1}^{n} \mathbb{V}_i + \sum_{i<j}^{n} \mathbb{V}_{ij} + \cdots + \mathbb{V}_{1,2,\ldots,n} \quad (2.10)$$

where:

$\mathbb{V}_i = \mathbb{V}(\mathbb{E}[Y|X_i])$*:* condition expectation

$\mathbb{V}_{ij} = \mathbb{V}(\mathbb{E}[Y|X_i, X_i]) - \mathbb{V}_i - \mathbb{V}_j$

The contribution of uncertain input parameters to variance of outputs is generally not known in advance, thus, sensitivity analysis (SA) was applied to analyze the influence of

individual uncertain inputs, in addition to an analysis of statistical parameters. The eventual goal is to know how uncertain input variables contribute to the variance of output, on their own, or through interactions with other parameters. This is useful for modeling personalization, for deciding which parameter needs to fix to its true value (input prioritization) or which parameter can fix within its uncertainty domain (input fixing).

For quantification, Sobol introduced total and main sensitivity indices:

- Main sensitivity indices: The main sensitivity indices also called the first-order Sobol sensitivity indices are the variance of the conditional expectation of the output Y given the value of an input X_i, normalized by the total variance:

$$S_i = \frac{\mathbb{V}\left[\mathbb{E}[Y|X_i]\right]}{\mathbb{V}[Y]} \tag{2.11}$$

where the index i varies from 1 to the number of uncertain input variables n, $1 \leq i \leq n$.

Especially, the main sensitivity index S_i represent the expected reduction in the total variance $\mathbb{V}[Y]$ when the input variable X_i can be fixed in its true value.

- Total index: includes the sensitivity of both first-order effects as well as the sensitivity due to interactions (covariance) between a given parameter X_i and all other parameters

$$S_{T_i} = 1 - \frac{\mathbb{V}\left[\mathbb{E}[Y|X_{-i}]\right]}{\mathbb{V}[Y]} \tag{2.12}$$

2.3 Geometry Modelling

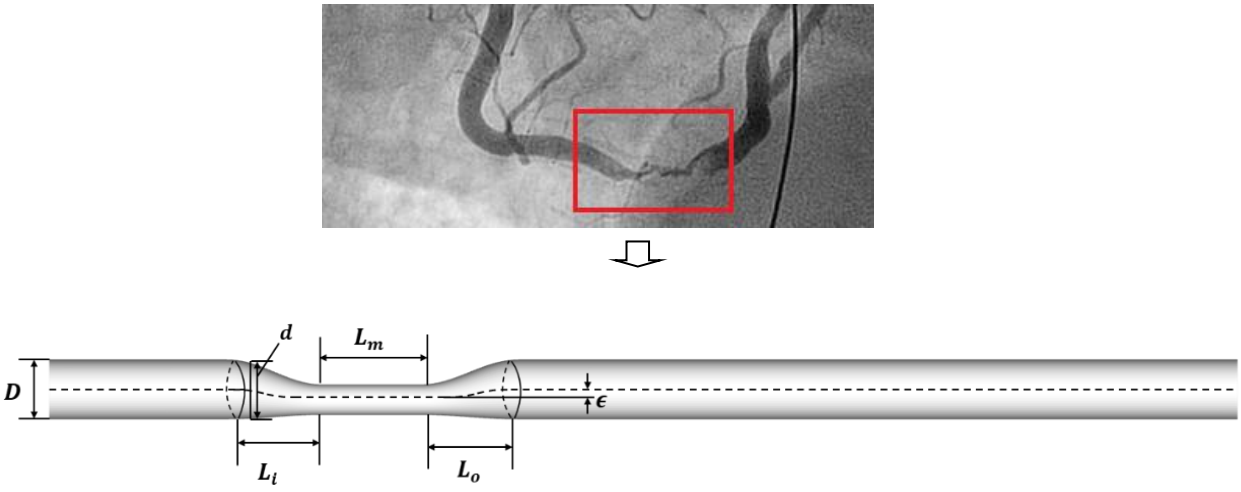

Figure 2.1 Geometry modeling from realistic stenosis to idealization geometry

By using the following equations, the actual geometry is modeled as an idealized geometry:

- For $z_0 \leq z \leq z_0 + L_i$

$$d(z) = D\left[1 - s_0 sin\frac{\pi}{2L_i}(z - z_0)\right] \tag{2.13}$$

$$e(z) = \epsilon s_0 \frac{D}{2} sin\frac{\pi}{2L_i}(z - z_0) \tag{2.14}$$

- For $z_0 + L_i \leq z \leq z_0 + L_i + L_m$

$$d(z) = D[1 - s_0] \tag{2.15}$$

$$e(z) = \epsilon s_0 \frac{D}{2} \tag{2.16}$$

- For $z_0 + L_i + L_m \leq z \leq z_0 + L_s$

$$d(z) = D\left[1 - s_0 cos\frac{\pi}{2L_o}(z - z_0 - L_i - L_m)\right] \tag{2.17}$$

$$e(z) = \epsilon s_0 \frac{D}{2} cos \frac{\pi}{2L_o}(z - z_0 - L_i - L_m) \tag{2.18}$$

- $L_s = L_i + L_m + L_o$
- $x(z) = \frac{d(z)}{2} cos\theta$
- $y(z) = e(z) + \frac{d(z)}{2} sin\theta$

where:

- D : the diameter of coronary
- L_i : the proximal region of stenosis
- L_m : the middle region of stenosis
- L_o : the distal region of stenosis
- ϵ : eccentricity
- s_0 : degree of stenosis

Figure 2.2 shows methods for calculating the degree of stenosis [21].

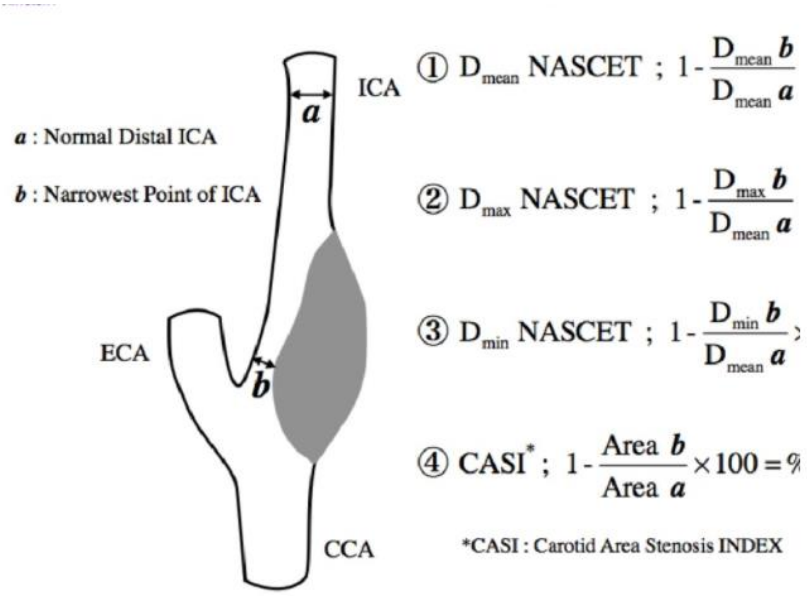

Figure 2.2 Methods to calculate the degree of stenosis

According to Myer-Cotton [22], the degree of stenosis can be classified as 4 grades.

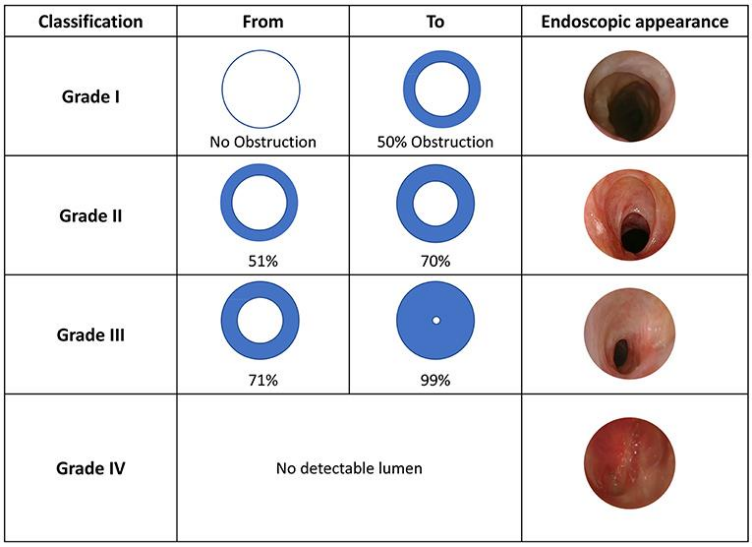

Figure 2.3 Classification of stenosis corresponds to the degree of stenosis

Grade I has the value of DS from 0% to 50%, Grade II from 51% to 70%, Grade III from 71% to 99%, and Grade IV no detectable lumen. In clinical application, Grade I is generally considered not serious, while Grade III has adverse effects on blood circulation. In this study, the degree of stenosis of 50% is considered for all cases.

2.4 Computational fluid dynamics model

By using the Galerkin finite element approach in combination with the P2-P1 scheme, the governing equations (e.g., Navier-Stoke equations) have ten velocity nodes and four pressure nodes (Figure 2.4). The shape functions of the velocity element are listed below in local coordinates:

$$(\xi, \zeta, \eta)\phi_1 = \xi(2\xi - 1) \tag{2.19}$$

$$\phi_2 = 4\xi\zeta \tag{2.20}$$

$$\phi_3 = \zeta(2\zeta - 1) \tag{2.21}$$

$$\phi_4 = 4\zeta\eta \tag{2.22}$$

$$\phi_5 = \eta(2\eta - 1) \tag{2.23}$$

$$\phi_6 = 4\xi\eta \tag{2.24}$$

$$\phi_7 = 4\xi(1 - s) \tag{2.25}$$

$$\phi_8 = 4\zeta(1 - s) \tag{2.26}$$

$$\phi_9 = 4\eta(1 - s) \tag{2.27}$$

$$\phi_{10} = (1 - 2s)(1 - s) \tag{2.28}$$

where s is equal to $\xi + \zeta + \eta$. The elemental pressure shape functions are given by:

$$\psi_1 = \xi \tag{2.29}$$

$$\psi_2 = \zeta \tag{2.30}$$

$$\psi_3 = \eta \tag{2.31}$$

$$\psi_4 = 1 - s \tag{2.32}$$

Using these shape functions, the velocity components u_i and the pressure p are written as:

$$u_i = \sum_{j=1}^{10} u_{i,j}\phi_j \tag{2.33}$$

$$p = \sum_{j=1}^{4} p_j\psi_j \tag{2.34}$$

$u_{i,j}$ is the *j*th component of the vector of nodal velocities $\{u_i\}$

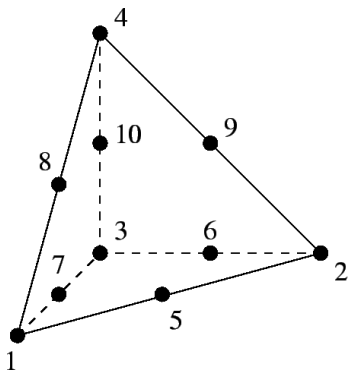

Figure 2.4 Tetrahedral Taylor-Hood elements

Usually, the boundary conditions in pipe flow simulation can be considered as the blood flow rate at the inlet and pressure at the outlet (Figure 2.5). However, it is not convenient when the pressure at the outlet is often lacked information, because determining the pressure value is complicated and is localized, depending on each location.

Figure 2.5 Conventional boundary conditions in pipe flow simulation

To overcome this problem, in blood flow simulation, the downstream boundary conditions can be modeled as the lumped parameter network (LPN) model or 0D model [2], which mimics electrical circuits.

Figure 2.6 Lumped parameter network model

where:

- R_a : coronary arterial resistance
- C_a : coronary arterial capacitance
- $R_{a-micro}$: coronary microvascular arterial resistance
- C_{im} : intra-myocardial capacitance
- P_{im} : intra-myocardial pressure
- $R_{v-micro}$: coronary micro vascular venous resistance
- R_v: coronary venous resistance

By adjusting the resistance value, the blood flow rate in the simulation can mimic the realistic conditions, while the capacitance value can shift the phase of blood flow. The parameter values of the LPN model are determined to match the characteristics of the LAD coronary.

2.5 Chaospy

Chaospy is a Python software toolbox for performing uncertainty quantification via polynomial chaos expansions and Monte Carlo simulation. Within the scope of Monte Carlo sampling and NIPC expansion, Chaospy has a competitive collection of methods, comparable to both Dakota and Turns [20].

Chaospy is used to generate random input samples as well as used to analyze UQ and SA values in this study.

3. EVALUATION OF NUMERICAL RESULTS

3.1 Single stenosed vessel

3.1.1 Geometry modeling

The mean values of geometry parameters in a single stenosed vessel are obtained from data of more than 400 patients [12, 23-25]. These mean values are listed in Table 3.1.

Table 3.1 Uncertain input variables for the single stenosed vessel.

No	Variables	Description	Value	Unit	Uncertainty
1	L_i	Proximal length	6.0	mm	5 %
2	L_m	Middle length	6.0	mm	5 %
3	L_o	Distal length	6.0	mm	5 %
4	D	Diameter	3.6	mm	5 %
5	DS	Degree of stenosis	50	%	5 %
6	P_{mean}	Pressure	90	mmHg	10 %
7	R_{ratio}	Resistance ratio	1	-	10 %

The single stenosed vessel has 7 uncertain input variables, corresponding to the geometry data and clinical parameters.

3.1.2 CFD validation

Figure 3.1 LPN model for single stenosed vessel

In the case of a single stenosed vessel, the LPN model is applied: the inlet boundary condition is aortic pressure, while the outlet is connected to a “circuit”.

The computational mesh is the second-order tetrahedral element, with 1,170,585 grid nodes. Mesh density is increased in the stenosis region. Stenosis is generated based on geometric data by using grid morphing technique.

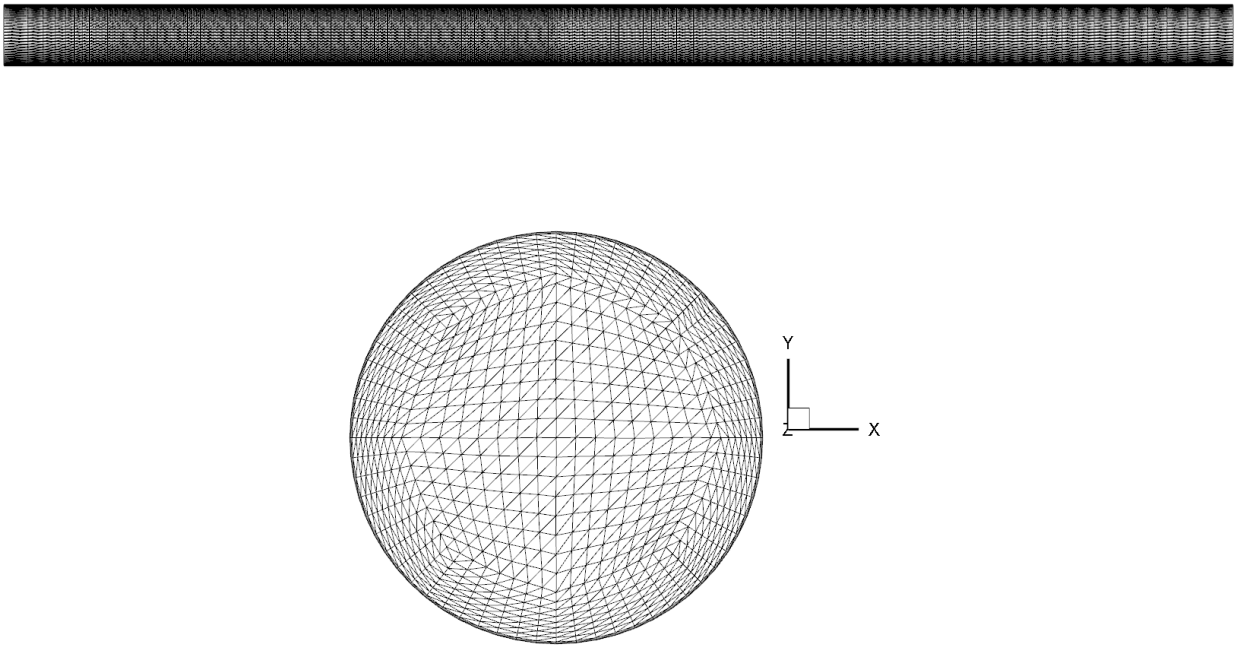

Figure 3.2 Grid for single stenosed vessel

The appropriate value for distal bed resistance at the outlet is obtained by using the trial-and-error method, different vascular resistance values are tested until the flow rate becomes same as pre-defined flow rate in the LAD coronary. The mean blood flow rate in LAD is 1ml/s.

Table 3.2 Boundary conditions for single stenosed vessel

Boundary conditions	**Flow characteristics**
$\boldsymbol{P_{mean} = 90\ mmHg}$	$Q_{mean} = 1.04\ ml/s$
$\boldsymbol{R_T = 120 \times 10^3\ Ba \cdot s/ml}$	$\Delta p_L = 85.3\ Pa\ \ (0.6398\ mmHg)$
$\boldsymbol{\mu = 0.0035\ Pa \cdot s}$	$Re_{mean} = 110$
$\boldsymbol{\rho = 1050\ kg/m^3}$	

The FFR value is evaluated in the hyperemia condition. To do this, the resistance at the outlet is divided by 4 compared to the baseline (normal) condition.

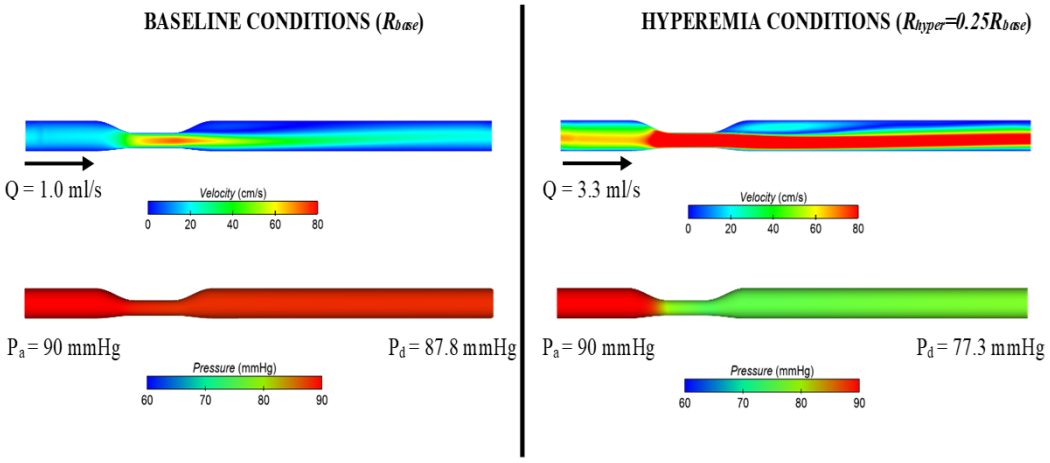

Figure 3.3 CFD results of single stenosed vessel created by mean values

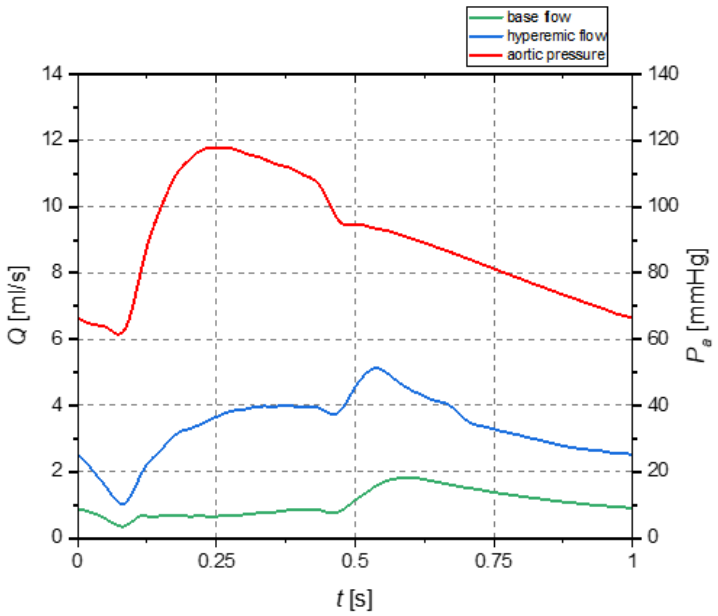

Figure 3.4 Flow characteristics of the single stenosed vessel by applying the LPM

The Reynolds number corresponds to the values described in Table 3.2 for baseline condition is $Re_{base} = \frac{4Q_{base}}{\pi D\upsilon} = \frac{4\times 1 cm^3/s}{3.14\times 0.36cm\times 0.035cm^2/s} = 101.10$, while the Reynolds number in the hyperemia condition is $Re_{hyp} = \frac{4Q_{hyp}}{\pi D\upsilon} = \frac{4\times 3.3 cm^3/s}{3.14\times 0.36cm\times 0.035cm^2/s} = 333.63$.

Small changes in the input parameters can lead to large differences in the output. Figure 3.6 is used to demonstrate this. It can be observed that the distribution of WSS or pressure in the single stenosed vessel has changed markedly.

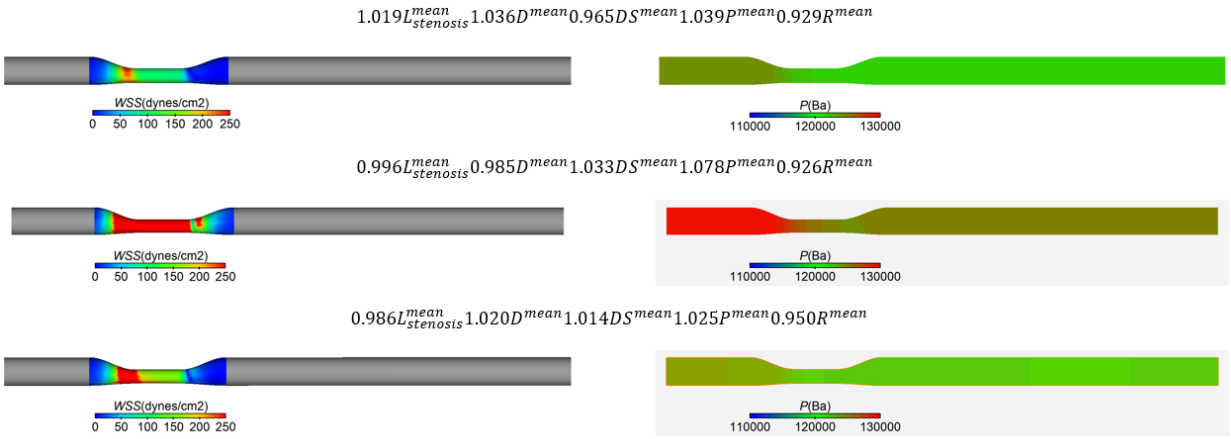

Figure 3.5 Differences in flow characteristics due to small errors in input variables in the single stenosed vessel model

3.1.3 UQ and SA for WSS and FFR

Figure 3.6 may justify that the application of UQ and SA is necessary, but this application is not easy, since the output values are also affected by the polynomial order and sample sizes chosen. To unravel how polynomial order and sample sizes affect the convergence of output results, we performed UQ and SA for WSS and FFR with different combinations of polynomial order (p) and sample sizes (n_{ps}).

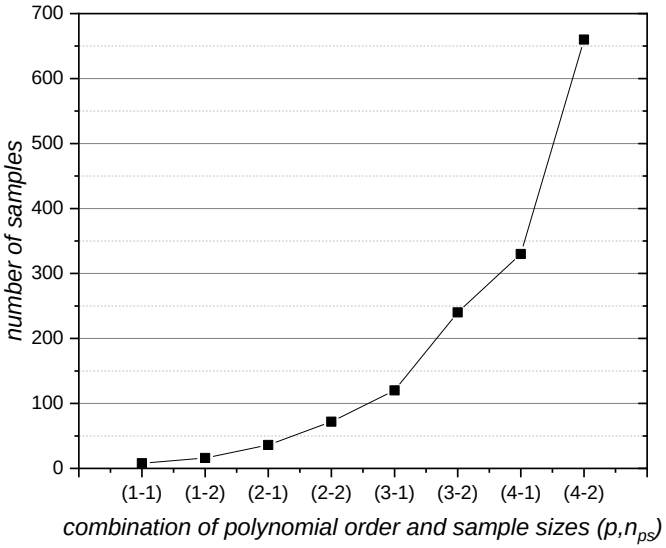

Figure 3.6 The number of samples required with different combination of polynomial order and sample sizes

With a total of 7 uncertain input variables, the number of samples required for UQ and SA raise incredibly alongside the increase in polynomial order and sample sizes.

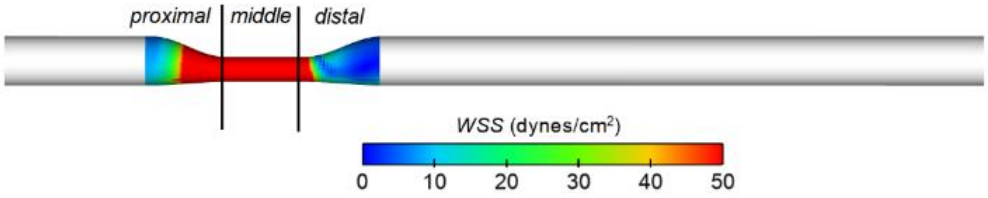

Figure 3.7 Distribution of WSS on the proximal, middle, and distal region of stenosis

Previous studies have observed a tendency to form high-risk plaque localized in high WSS regions in the stenotic proximal segments [8], thus the higher WSS in the proximal segment has an important role in the prediction of myocardial infarction.

We performed UQ and SA for averaged proximal WSS $(AWSS_{prox})$ respect to the uncertain input variables $(L_i, L_m, L_o, D, DS, P_a, R)$. To evaluate the convergence of results using the simulation model, a comparison of the expected value, the coefficient of variance

$\left(CV = \frac{\sigma}{\mathbb{E}}\right)$, and the total sensitivity index (S_i^T) of each combination (p, n_{ps}) are performed. These comparisons indicated the optimal choice for the combination (p, n_{ps})..

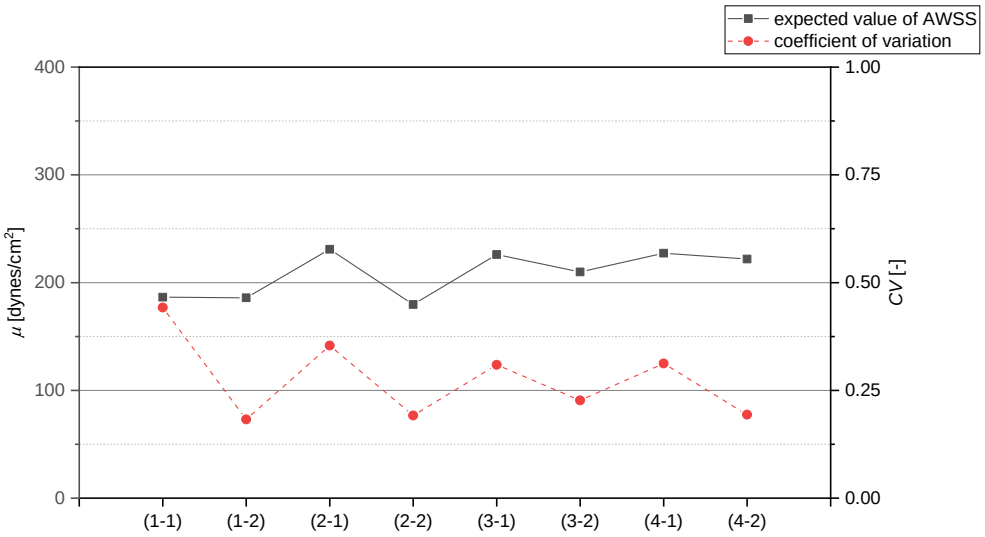

Figure 3.8 Variation of the mean value of $AWSS_{prox}$ and CV corresponding to combination $(p - n_{ps})$

Figure 3.9 shows the expected value (μ-black points) and coefficient of variation (CV-red points) of $AWSS_{prox}$ for each combination of polynomial order (p) and sample sizes (n_{ps}). We observed that from the combination $(p = 3, n_{ps} = 1)$ onwards, the discrepancy in the μ is small, more precisely, the difference between the maximum and the minimum expected value $\left(\frac{\mu_{max} - \mu_{min}}{\mu_{mean}} \times 100\%\right)$ is 8.1% while the CV value fluctuates around 0.25.

We not only compare μ and CV values but also the total sensitivity indices (S_i^T), which are illustrated in Figure 3.10. We observed that from the combination $(p = 3, n_{ps} = 2)$ onwards, the behavior of S_i^T values are similar. Intuitively, from the trend of S_i^T, we observed the S_i^T value of diameter (D) with combinations $(p = 3, n_{ps} = 1)$ backward having a much different behavior than the combination $(p = 3, n_{ps} = 2)$ onwards, which seems to vanish.

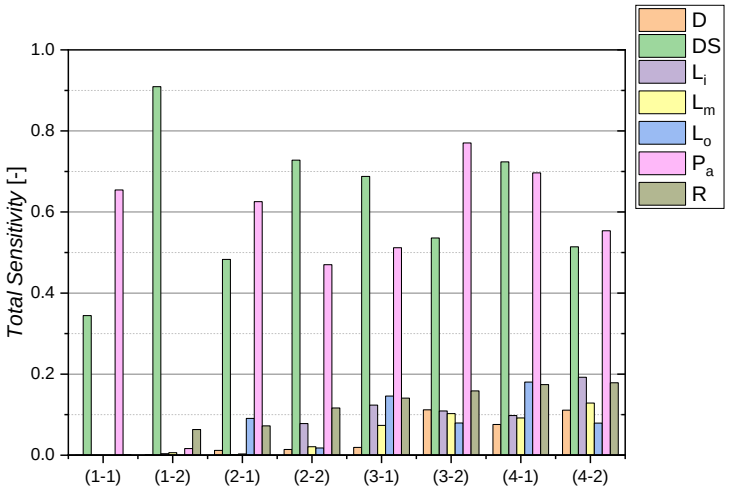

Figure 3.9 Total sensitivity of uncertain variables in the single stenosed vessel model

From the above comparisons, we found that combination of the third-order polynomial with the twice required sample $(p = 3, n_{ps} = 2)$ can reach the similar results in UQ and SA as well as higher combinations, with the computational cost-saving (the number of samples required is 240 compared to 660 of the combination $p = 4, n_{ps} = 2$). In addition to comparing the UQ and SA indices, we demonstrate the probability distribution for each combination in Figure 8. The distribution, plotted for 10,000 counts, has the same shape for the combination $(p = 3, n_{ps} = 1)$ onwards, is asymmetric with a longer tail towards the higher proximal averaged WSS values.

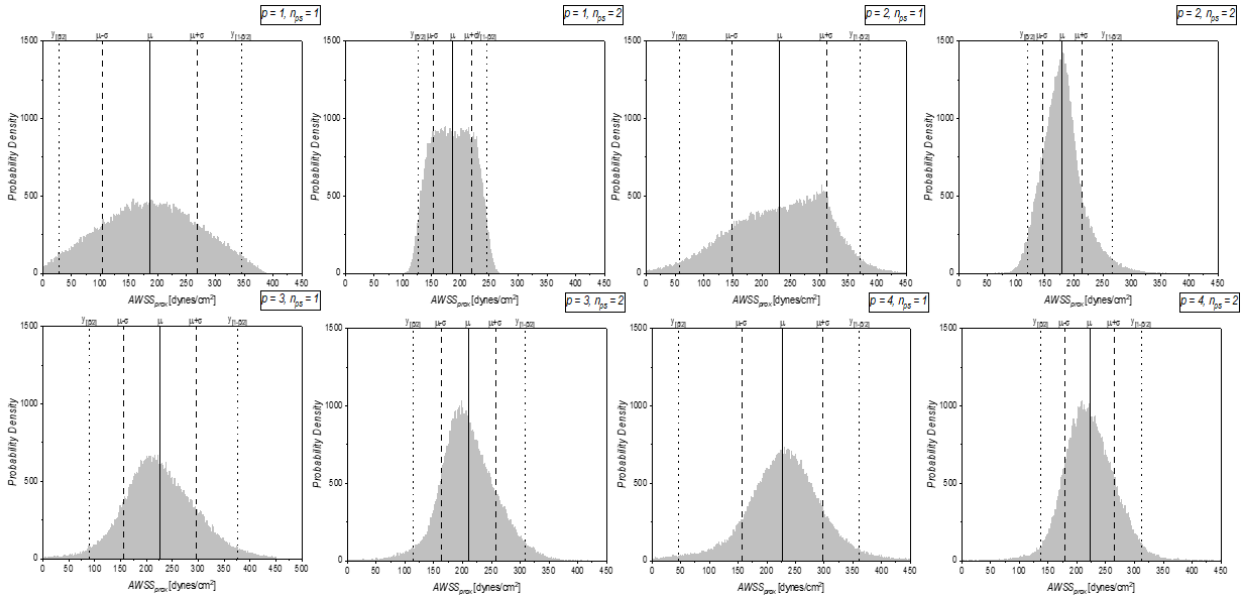

Figure 3.10 Density distribution of $AWSS_{prox}$ corresponding to combination $(p - n_{ps})$

We showed that a polynomial degree of 3 $(p = 3)$ with Latin Hypercube sampling and samples sizes $(n_{ps} = 2)$ was capable of UQ and SA for WSS in the hypothesis case. Table 3.3 gives the computation time associated with each combination (p, n_{ps}). As can be seen from this table, the time required to complete the simulations for a combination $(p = 3, n_{ps} = 2)$ are 100 hours, whereas for a combination $(p = 4, n_{ps} = 2)$, it took 275 hours to finish the simulation. Thus, the combination $(p = 3, n_{ps} = 2)$ is the optimal choice to do UQ and SA in this numerical model with a significantly lower computation cost. However, in this study, we examined the influence of the uncertain input variables on the variance of $AWSS_{prox}$ by calculating the main sensitivity indices S_i on the fourth-order polynomial and twice the required number of samples $(p = 4, n_{ps} = 2)$. As can be seen from Figure 3.12, the degree of stenosis (DS) has the highest main sensitivity index, followed by mean aortic pressure P_a, while the remaining variables have low influence $(\leq 5\%)$. More precisely, these sensitivity indices illustrate that if DS and P_a could be fixed to their true values, the uncertainty in $AWSS_{prox}$would be reduced by 25% and 9.5%, respectively.

Table 3.3 Computation time corresponding to combination ($p - n_{ps}$)

	(Polynomial order p, samples sizes n_{ps})		
	(3,2)	(4,1)	(4,2)
number of samples	240	330	660
computation time (hours)	100	137.5	275

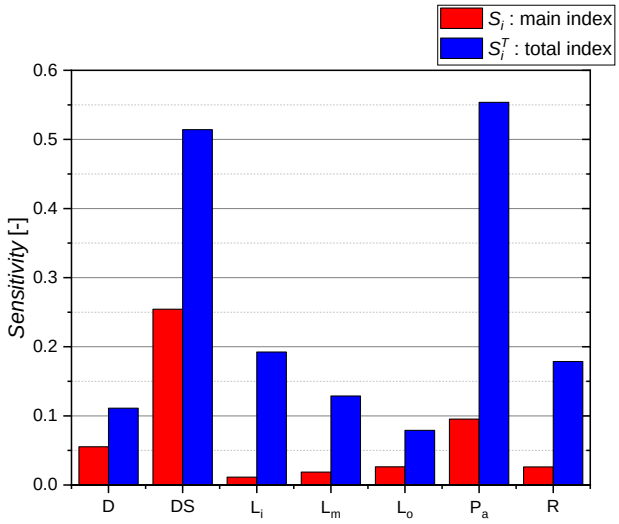

Figure 3.11 The sensitivity indices for the computational model of $AWSS_{prox}$

Total sensitivity indices S_i^T are used to consider the interaction effects between the uncertainty input variables. If the total sensitivity index value of a variable is almost zero, there is no association between this parameter and all other parameters, so this parameter can be fixed within its uncertainty domain, as they are not important when $S_i^T \approx 0$. Variable P_a has the highest difference between S_i^T and S_i, about 46%, while the S_i^T value of the variable

L_o is only 0.07, which means if we can fix the variables $(L_i, L_m, D, DS, P_a, R)$ will only leave 7% uncertain $AWSS_{prox}$. Therefore, variable L_o could be fixed within its uncertainty domain.

In the computational model of the FFR, the uncertain input variables have the same error in the WSS case, however, the coronary resistance value at the output decreased 4 times compared with the baseline condition. The regression NIPC method and the Latin Hypercube sampling technique were applied to evaluate the uncertainty of the FFR value. As same as the UQ and SA for WSS, fourth-order polynomial $p = 4$with the sample sizes $n_{ps} = 2$ were used to generate the surrogate model for FFR, the purpose is to evaluate the effect of the uncertain input variables on the variance of the FFR, then compare it with the WSS case and find out the difference.

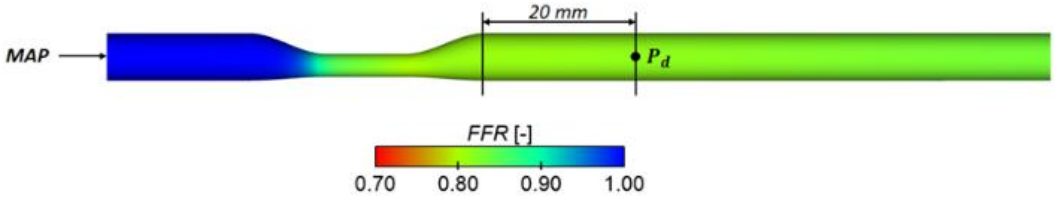

Figure 3.12 Schematic for estimating FFR value in the single stenosed vessel

We calculated the statistical characteristics of the probability density of the FFR for 10,000 counts, including expected values, variance, and the 95% confident interval. In Figure 3.14, we observed that the FFR density distribution presents an asymmetry, with a longer tail towards the lower FFR values.

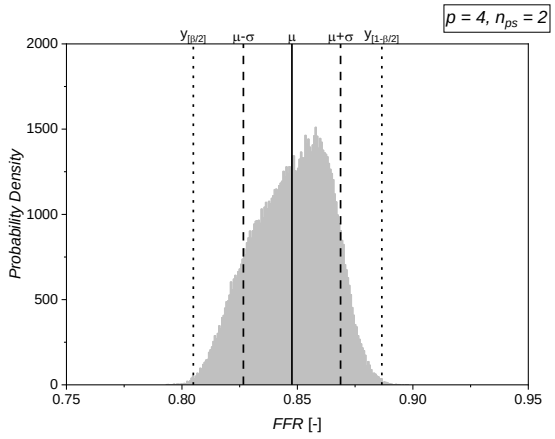

Figure 3.13 The probability density for uncertain FFR

As can be seen from Figure 3.15, the variables that have significant influences on the uncertainty of the FFR simulation model are diameter (D), degree of stenosis (DS), and coronary resistance (R). More specifically, the main sensitivity index values of D, DS, R are 0.31, 0.41, and 0.24, respectively, which means that if we could correct the DS value to its true value, the variance of FFR could be reduced by up to 41%, similarly for D and R. Whereas the influence of the length variables (L_i, L_m, l_o) seem to be zero, and the influence of the mean aortic pressure (P_a) is smaller than 5%. There was no interaction between variables in the FFR simulation model since the difference between S_i^T and S_i is small.

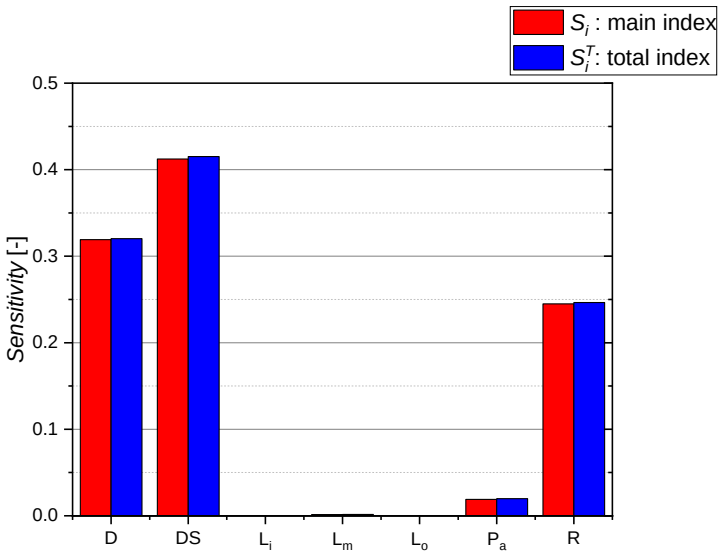

Figure 3.14 The sensitivity indices for the computational model of FFR

3.2 Tandem stenosed vessel

3.2.1 Geometry modeling

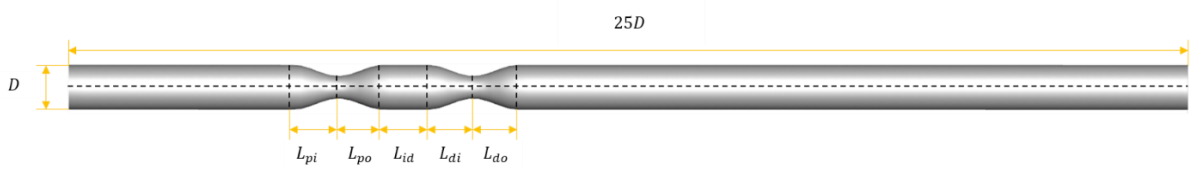

Figure 3.15 Geometrical scheme of the tandem stenosed vessel

In the case of a tandem stenosed vessel, we applied the same boundary conditions in the experiment of Huh et al. [11]. With the Reynolds value used of 187 and the distance between two stenoses only D, the flow after the distal stenosis is the laminar.

Table 3.4 Uncertain input variables for tandem stenosed vessel

No	Variables	Description	Mean Value	Unit	Uncertainty
1	D	Arterial diameter	8.0	mm	5 %
2	DS_p	Proximal stenosis severity	50	%	5 %
3	L_{pi}	Proximal in-length	8.0	mm	5 %
4	L_{po}	Proximal out-length	8.0	mm	5 %
5	L_{id}	Interspacing distance	8.0	mm	5 %
6	DS_d	Distal stenosis severity	50	%	5 %
7	L_{di}	Distal in-length	8.0	mm	5 %
8	L_{do}	Distal out-length	8.0	mm	5 %
9	Q	Flow rate	4.11	ml/s	10 %

3.2.2 CFD validation

Numerical simulations were conducted by using well validated in-house code (PADAM) and compared with the experimental results of Hut et al. [11] for validation. Additional CFD simulations were performing using OpenFOAM for further validation with the same boundary conditions.

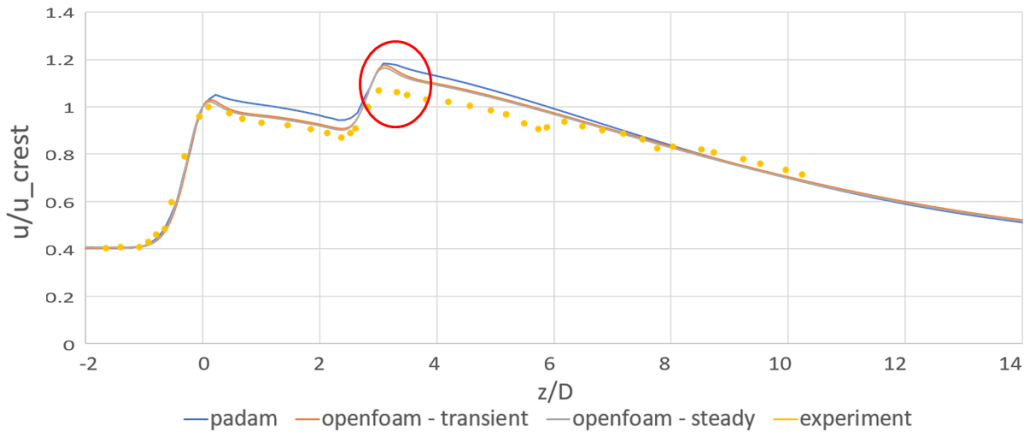

Figure 3.16 Comparison of centerline velocity between CFD (PADAM and OpenFOAM) and experiment [11].

Figure 3.17 shows the centerline axial velocity calculated by PADAM is in good agreement with the OpenFOAM data, however, there is somewhat discrepancy between experiment and CFD results at the crest position of distal stenosis, which is around 10% of the velocity.

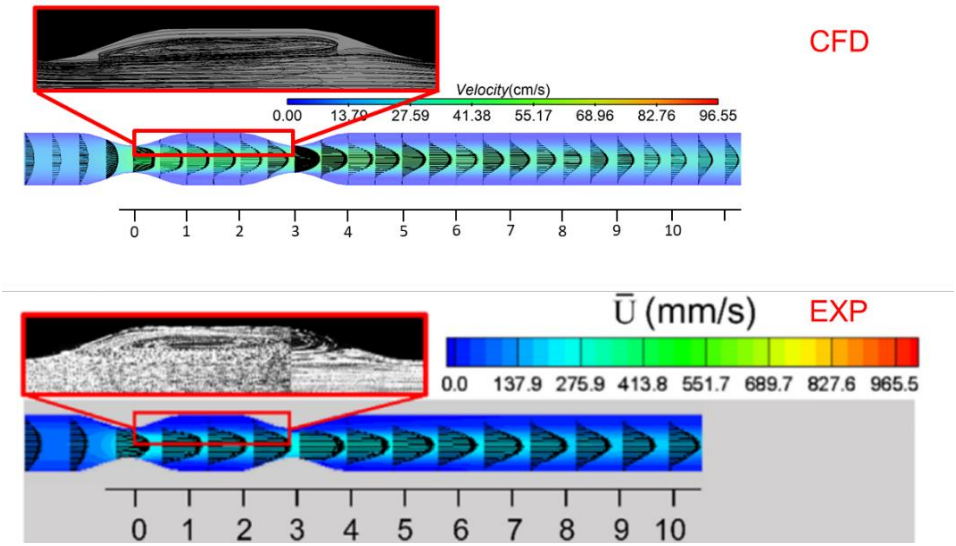

Figure 3.17 Comparison of flow distribution and recirculation between CFD and experiment results

Figure 3.18 illustrates the distribution of the recirculation zone between the CFD results (using PADAM) and the experiment [11]. The center of the recirculation zone is around the middle of zones $1D - 2D$.

It was observed that changing the input values by a small interval creates significant change in the output as shown in Figure 3.19.

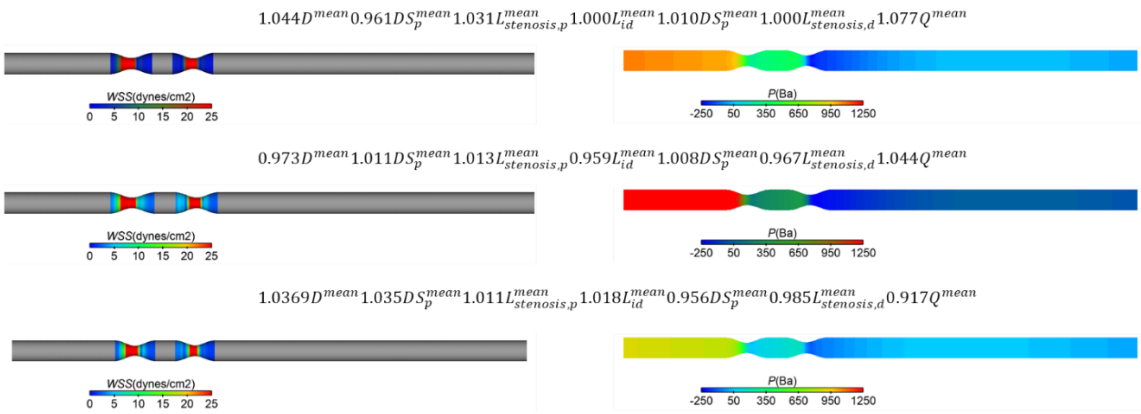

Figure 3.18 Differences in flow characteristics due to small errors in input variables in the tandem stenosed vessel model

3.2.3 UQ and SA for WSS and FFR

A total of 9 uncertain input variables were considered in the tandem stenosed vessel model, we used fourth-order polynomial ($p = 4$) and double the required number of sample ($n_{ps} = 2$) to perform UQ and SA. Thus, the total number of samples to be used is 1430. To generate the stochastic input sample set, we used the Latin Hypercube sampling rule, assuming the uniform distribution.

From UQ analysis, we found that the mean $\pm$ std value of the centerline velocity of the numerical simulation covers the experimental results conducted by Hut et al. [11]. This shows that the CFD outputs can be biased by more than 10% with only 5% (or 10%) variation in inputs.

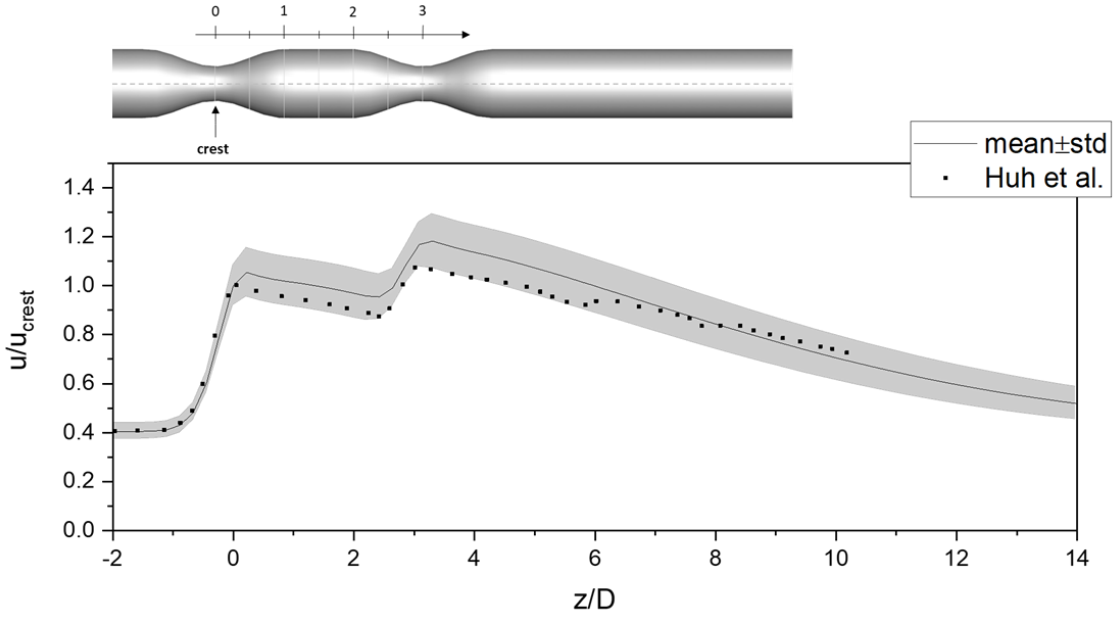

Figure 3.19 Mean and standard deviation of the centerline velocity by UQ

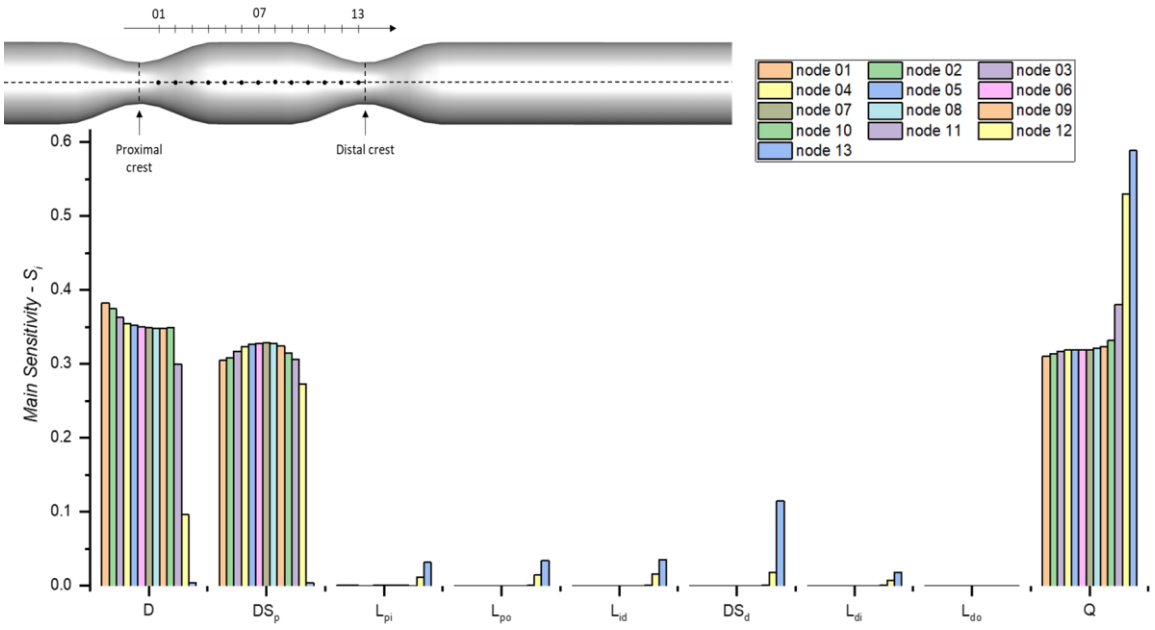

Figure 3.20 The main sensitivity indices for the computational model of centerline velocity

Performing SA, we investigated the influences of the uncertain input variables on the centerline velocity at 13 equally spaced points between the two serial stenoses. Based on the main sensitivity index (S_i) values, we found that the influence of arterial diameter (D) on the variance of the centerline velocity decreased from the proximal to the distal crest, whereas the contribution of blood flow rate (Q) increased. Significant changes in the contributions of these variables occurred at a location close to the distal crest.

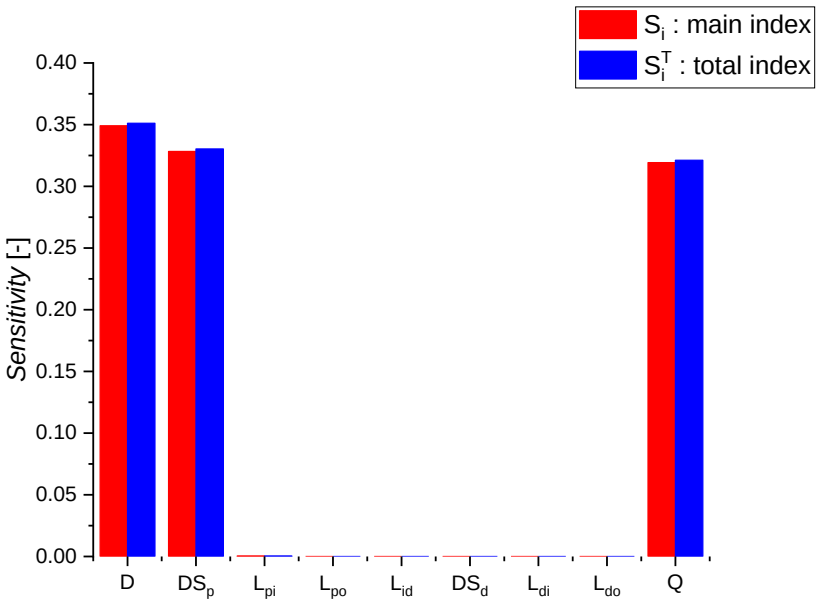

Figure 3.21 The sensitivity indices for the centerline velocity at node 07

There is no interaction between variables in the FFR simulation model since the difference between S_i^T and S_i is small.

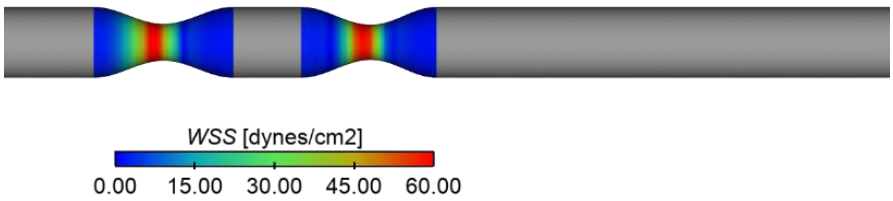

Figure 3.22 Distribution of WSS on the proximal and the distal stenosis

We calculated the statistical characteristics of the probability density of the WSS for 10,000 counts, including expected values, variance, and the 95% confident interval. We observed that the WSS density distribution on both regions (proximal and distal stenosis) presents an asymmetry, with a longer tail towards the higher WSS values. We also found that the mean WSS value in the distal stenosis was lower than in proximal stenosis. This can be explained by the fact that the stenosis in the distal region produces a larger centerline velocity

than in the proximal region, consequently, the gradient of velocity near the blood vessel wall is smaller.

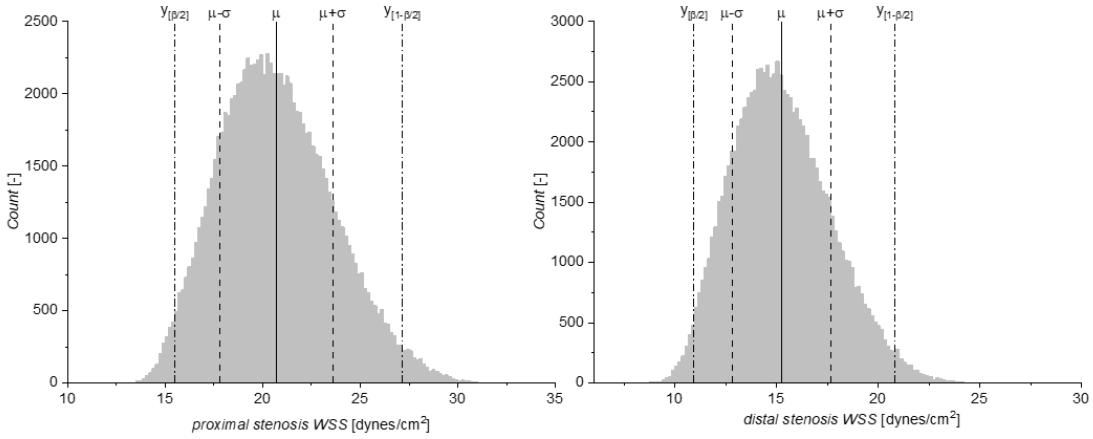

Figure 3.23 The probability density for uncertain WSS (left for proximal stenosis, right for distal stenosis)

Figure 3.25 shows a comparison of the main sensitivity index and total sensitivity index values. Similar as centerline velocity, the impact of uncertain input variables on the variation of WSS depends on the location. For WSS in the proximal stenosis region, arterial diameter (D), degree of proximal stenosis (DS_p), and blood flow rate (Q) significantly contribute to the variation, which are 35%, 29%, and 30% respectively. Meanwhile, in the distal region, the uncertainties of arterial diameter (D), degree of distal stenosis (DS_d), and blood flow rate (Q), have the intuitive influence on the variation of distal WSS, which are 28%, 45%, and 18% respectively. There was only minor interaction between input variables in the FFR simulation model since the difference between S_i^T and S_i is small.

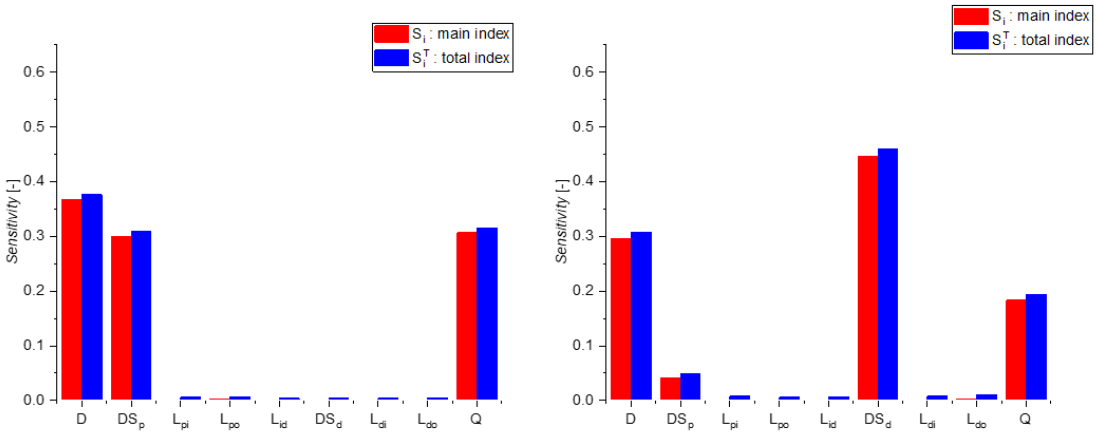

Figure 3.24 The sensitivity indices for uncertain WSS (left for proximal stenosis, right for distal stenosis)

For the pressure distribution, we found that variation of pressure in the downstream of distal stenosis was lower than in the upstream of the proximal stenosis region. Similarly, the influence of uncertain input variables on the variation of pressure also depends on the location. For downstream of distal stenosis, arterial diameter (D), degree of distal stenosis (DS_d) and blood flow rate (Q) significantly contribute to the variation of pressure. However, the influence of the rest of the variables seems to vanish.

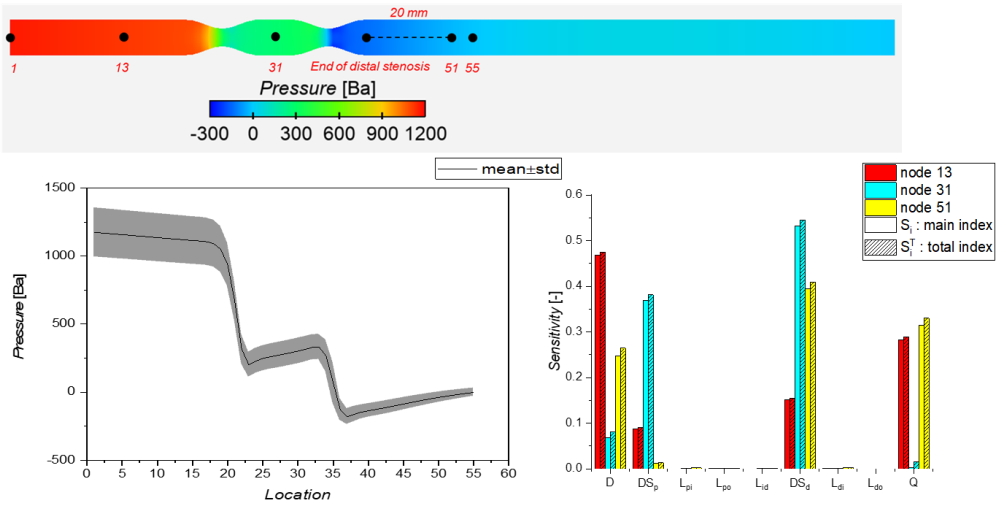

Figure 3.25 The uncertain of pressure in the tandem stenosed vessel

4. CONCLUSION

In this study, we performed UQ and SA for idealized single stenosed vessels and tandem stenosed vessels with uncertain input variables. We have shown that UQ and SA are necessary since the variability of the output is generally high under the current assumption of the idealized model.

For the single stenosed model: By comparing statistical parameters and sensitivity indices, we found that using third-order polynomial $p = 3$ coupled with sample sizes $n_{ps} = 2$ was predictable the effect of the uncertain input variables as well as the distribution of uncertain outputs. By SA, we found that the influence of parameters on each hemodynamic index is different, the uncertainty of the degree of stenosis DS and mean aortic pressure P_a need to be measured accurately to improve the computational WSS, while the normal diameter D, degree of stenosis DS and coronary resistance R significantly contribute to the variance of FFR. With the WSS value in the proximal region, accurately predicting its outcome is not, as its approximately 95% confident interval ranges from 150 dynes/cm2 to 325 dynes/cm2 with a mean value of 225 dynes/cm2, while the value of FFR has about 95% confidence interval compared to mean relatively small value, about 95% confidence interval 0.815 to 0.88, while mean value is 0.84. However, these values are all within the dangerous threshold by medical standards.

For the tandem stenosed model: We have performed UQ and SA for tandem stenosed vessels according to the experimental model of Huh et al. [11], through which we found that it is necessary to strictly control the input values when small errors in inputs can lead to dramatically change in output. About the effect of uncertain input variables, the impact of parameters on proximal and distal stenosis is different. For proximal stenosis, these parameters should be improved: diameter, degree of proximal stenosis, blood flow rate.

Meanwhile, parameters such as diameter, degree of distal stenosis and blood flow rate need to be paid attention to if we want to estimate more accurate distal stenosis WSS. We also have the same comment as Huh et al. [11] that there is no effect of degree of distal stenosis on the downstream flow of proximal stenosis.

5. LIMITATIONS AND FUTURE WORKS

Limitations:

In this study, we assume that all the uncertain inputs are not related to each other, which is not always true in cardiovascular applications. However, the relationship between these variables is almost unknown.

We performed UQ and SA only on idealized stenosis geometry with uniformly distributed random parameters. In fact, the coronary geometries are extremely complex, and the parameters are uncertain in terms of time or space.

Future works:

The degree of stenosis can reach Grade III (71% to 99%), analysis for these cases is necessary to obtain an overview for the diagnosis of CAD.

We sequentially performed the UQ and SA for the stochastic sample set, when the sample set becomes large due to an increase in input parameters or the requirement to use higher polynomial order, the computation time also increases. Applying deep learning can help us overcome this.

REFERENCE

1. Organiztion, W.H., in *who.int*. 2019.

2. Sankaran, S., Esmaily Moghadam, M., Kahn, A.M., Tseng, E.E., Guccione, J.M., and Marsden, A.L., *Patient-specific multiscale modeling of blood flow for coronary artery bypass graft surgery.* Ann Biomed Eng, 2012. **40**(10): p. 2228-2242.

3. Kim, H.J., Vignon-Clementel, I.E., Coogan, J.S., Figueroa, C.A., Jansen, K.E., and Taylor, C.A., *Patient-specific modeling of blood flow and pressure in human coronary arteries.* Ann Biomed Eng, 2010. **38**(10): p. 3195-3209.

4. Kolli, K.K., Min, J.K., Ha, S., Soohoo, H., and Xiong, G., *Effect of Varying Hemodynamic and Vascular Conditions on Fractional Flow Reserve: An In Vitro Study.* J Am Heart Assoc, 2016. **5**(7).

5. Cheruvu, P.K., Finn, A.V., Gardner, C., Caplan, J., Goldstein, J., Stone, G.W., Virmani, R., and Muller, J.E., *Frequency and distribution of thin-cap fibroatheroma and ruptured plaques in human coronary arteries: a pathologic study.* J Am Coll Cardiol, 2007. **50**(10): p. 940-949.

6. Corban, M.T., Eshtehardi, P., Suo, J., McDaniel, M.C., Timmins, L.H., Rassoul-Arzrumly, E., Maynard, C., Mekonnen, G., King, S., 3rd, Quyyumi, A.A., Giddens, D.P., and Samady, H., *Combination of plaque burden, wall shear stress, and plaque phenotype has incremental value for prediction of coronary atherosclerotic plaque progression and vulnerability.* Atherosclerosis, 2014. **232**(2): p. 271-276.

7. Stone, P.H., Coskun, A.U., Kinlay, S., Clark, M.E., Sonka, M., Wahle, A., Ilegbusi, O.J., Yeghiazarians, Y., Popma, J.J., Orav, J., Kuntz, R.E., and Feldman, C.L., *Effect of endothelial shear stress on the progression of coronary artery disease, vascular remodeling,*

and in-stent restenosis in humans: in vivo 6-month follow-up study. Circulation, 2003. **108**(4): p. 438-444.

8. Slager, C.J., Wentzel, J.J., Gijsen, F.J., Thury, A., van der Wal, A.C., Schaar, J.A., and Serruys, P.W., *The role of shear stress in the destabilization of vulnerable plaques and related therapeutic implications.* Nat Clin Pract Cardiovasc Med, 2005. **2**(9): p. 456-464.

9. DL, F., *Certain chemorheologic considerations regarding the blood vascular interface with particular reference to coronary artery disease.* Circulation, 1969. **40**: p. 38–57.

10. Zarins, C.K., Giddens, D.P., Bharadvaj, B.K., Sottiurai, V.S., Mabon, R.F., and Glagov, S., *Carotid bifurcation atherosclerosis. Quantitative correlation of plaque localization with flow velocity profiles and wall shear stress.* Circ Res, 1983. **53**(4): p. 502-514.

11. Huh, H.K., Choi, W.R., Ha, H., and Lee, S.J., *Flow characteristics around proximal and distal stenoses in a series of tandem stenosed vessels.* J Biomech, 2016. **49**(13): p. 2960-2967.

12. Eck, V.G., Donders, W.P., Sturdy, J., Feinberg, J., Delhaas, T., Hellevik, L.R., and Huberts, W., *A guide to uncertainty quantification and sensitivity analysis for cardiovascular applications.* Int J Numer Method Biomed Eng, 2016. **32**(8).

13. Sankaran, S. and Marsden, A.L., *A stochastic collocation method for uncertainty quantification and propagation in cardiovascular simulations.* J Biomech Eng, 2011. **133**(3): p. 031001.

14. Fishman, G., *Monte Carlo: Concepts, Algorithms, and Applications*. 1996: Springer.

15. Hosder, S. and Maddalena, L., *Non-Intrusive Polynomial Chaos for the Stochastic CFD Study of a Supersonic Pressure Probe*, in *47th AIAA Aerospace Sciences Meeting including The New Horizons Forum and Aerospace Exposition*. 2009, American Institute of Aeronautics and Astronautics.

16. Xiu, D. and Hesthaven, J.S., *High-Order Collocation Methods for Differential Equations with Random Inputs.* SIAM Journal on Scientific Computing, 2005. **27**(3): p. 1118-1139.

17. Huberts, W., Donders, W.P., Delhaas, T., and van de Vosse, F.N., *Applicability of the polynomial chaos expansion method for personalization of a cardiovascular pulse wave propagation model.* Int J Numer Method Biomed Eng, 2014. **30**(12): p. 1679-1704.

18. Eldred, M., Webster, C., and Constantine, P., *Evaluation of Non-Intrusive Approaches for Wiener-Askey Generalized Polynomial Chaos,* in *49th AIAA/ASME/ASCE/AHS/ASC Structures, Structural Dynamics, and Materials Conference, 16th AIAA/ASME/AHS Adaptive Structures Conference,10th AIAA Non-Deterministic Approaches Conference, 9th AIAA Gossamer Spacecraft Forum, 4th AIAA Multidisciplinary Design Optimization Specialists Conference*. 2008, American Institute of Aeronautics and Astronautics.

19. Xiu, D., *Numerical Methods for Stochastic Computations: A Spectral Method Approach*. 2010: Princeton University Press.

20. Feinberg, J. and Langtangen, H.P., *Chaospy: An open source tool for designing methods of uncertainty quantification.* Journal of Computational Science, 2015. **11**: p. 46-57.

21. JM, U.K.-I., Trivedi, R.A., Cross, J.J., Higgins, N.J., Hollingworth, W., Graves, M., Joubert, I., Kirkpatrick, P.J., Antoun, N.M., and Gillard, J.H., *Measuring carotid stenosis on contrast-enhanced magnetic resonance angiography: diagnostic performance and reproducibility of 3 different methods.* Stroke, 2004. **35**(9): p. 2083-2088.

22. Myer, C.M., 3rd, O'Connor, D.M., and Cotton, R.T., *Proposed grading system for subglottic stenosis based on endotracheal tube sizes.* Ann Otol Rhinol Laryngol, 1994. **103**(4 Pt 1): p. 319-323.

23. Koo, B.K., Erglis, A., Doh, J.H., Daniels, D.V., Jegere, S., Kim, H.S., Dunning, A., DeFrance, T., Lansky, A., Leipsic, J., and Min, J.K., *Diagnosis of ischemia-causing coronary*

stenoses by noninvasive fractional flow reserve computed from coronary computed tomographic angiograms. Results from the prospective multicenter DISCOVER-FLOW (Diagnosis of Ischemia-Causing Stenoses Obtained Via Noninvasive Fractional Flow Reserve) study. J Am Coll Cardiol, 2011. **58**(19): p. 1989-1997.

24. Sankardas, M.A., McEniery, P., Aroney, C., Holt, G., Cameron, J., Garrahy, P., Dare, A., and Bett, N., *Directional coronary atherectomy for lesions of the proximal left anterior descending artery: initial clinical results, complications and histopathological findings.* Aust N Z J Med, 1995. **25**(6): p. 676-680.

25. Wieneke, H., Haude, M., Ge, J., Altmann, C., Kaiser, S., Baumgart, D., von Birgelen, C., Welge, D., and Erbel, R., *Corrected coronary flow velocity reserve: a new concept for assessing coronary perfusion.* Journal of the American College of Cardiology, 2000. **35**(7): p. 1713-1720.